Available online at www.sciencedirect.com
ScienceDirect
Journal of Power Sources 166 (2007) 331–336
JOURNAL OF POWER SOURCES
www.elsevier.com/locate/jpowsour

Short communication

Improving the performance of PtRu/C catalysts for methanol oxidation by sensitization and activation treatment

Jing Zhu, Yi Su, Fangyi Cheng, Jun Chen *

Institute of New Energy Material Chemistry, Nankai University, Tianjin 300071, PR China

Received 22 December 2006; received in revised form 29 January 2007; accepted 30 January 2007
Available online 6 February 2007

Abstract

PtRu/C anode electrocatalysts for direct methanol fuel cells (DMFCs) have been prepared by electroless deposition with the pretreatment of Sn^{2+}/Sn^{4+} sensitization and Pd activation. The as-prepared catalysts were composed of well dispersed PtRu alloy nanoparticles with relatively homogeneous size distribution, which were characterized by instrumental analyses, such as XRD, TEM, HRTEM and EDX. Electrochemical measurements demonstrated that the PtRu/C catalysts obtained with sensitizing and activating pretreatment exhibited an enhanced peak current density of 34% for methanol electrooxidation as compared to that synthesized without pretreatment.

Keywords: DMFCs; Pt-Ru catalyst; Sensitization; Activation

1. Introduction

In recent years, direct methanol fuel cells (DMFCs) have been considered to be promising alternative power sources for electric vehicles, portable electronic devices and mobile applications [1,2]. However, the poor activity and low utilization efficiency of noble metal catalysts pose a challenge to the development of DMFC because of the sluggish kinetic rate of methanol oxidation, therefore highly active electrocatalysts are required. Up to now, considerable efforts have been made on developing Pt-based alloy catalysts for methanol electrooxidation [3–7]. Among various investigated catalysts, bimetallic PtRu supported on carbon substrate exhibit the most prominent catalytic capability because the neighboring Ru atoms form oxygenated species at lower potentials compared with pure Pt. Accordingly, their presence promotes the oxidation of poisonous intermediate, CO, which is prone to be absorbed on metal surface. The methanol oxidation on Pt-Ru has been commonly explained by the bifunctional mechanism [8] and/or electronic (ligand) effect [9].

On the other hand, the correlation between the synthetic strategy and the property of catalysts has always been an attractive topic for both scientific and technological research. Various methods have been developed to prepare well dispersed PtRu catalysts in small particle size and narrow size distribution, such as organic sol method using methanol as solvent [10], fabricating colloidal nanoalloys in surfactant–organic solvent system [11], as well as applying polymers, quaternary ammonium salts or surfactants as protective agents [12]. Electroless deposition with pretreatment of sensitization and activation is an effective and widely used route to deposit metals on substrates. For example, silver nanoparticles deposited on polystyrene beads have been fabricated through this route [13]. Moreover, Pt nanoparticles coated on the walls of carbon nanotubes were also prepared and employed as electrocatalysts for H_2–O_2 fuel cells [14]. However, to the best of our knowledge, few reports have focused on the synthesis of carbon supported PtRu catalysts for methanol oxidation by using the electroless deposition method with the pretreatment of sensitization and activation.

Herein, we report on the preparation of well dispersed PtRu/C catalysts through an electroless deposition route with sensitizing and activating pretreatment. The as-synthesized catalysts showed that the pretreatment of sensitization and activation had prominent effect on the dispersion and size homogeneity of catalyst particles. Electrochemical investigations indicated that PtRu/C catalysts obtained by electroless depositioin with pretreatment have superior catalytic activities for methanol electrooxidation as compared to that synthesized without pretreatment. The fine dispersion, moderate particle size and narrow

* Corresponding author. Tel.: +86 22 23506808; fax: +86 22 23509118.
E-mail address: chenabc@nankai.edu.cn (J. Chen).

0378-7753/$ – see front matter © 2007 Elsevier B.V. All rights reserved.
doi:10.1016/j.jpowsour.2007.01.087

size distribution of the obtained catalyst particles led to favorable catalytic characteristics. The present results may shed some light on improving the catalytic performance for DMFCs.

2. Experimental

2.1. Catalyst preparation

H_2PtCl_6, $RuCl_3$ and $PdCl_2$ were purchased from Sino-Platinum Metals Co., Ltd. Vulcan XC-72 (Cabot) carbon black with a specific surface area of 250 $m^2\,g^{-1}$ was applied as the support. Nafion solution (5 wt.%) was purchased from Aldrich. All the other chemicals were of analytical grade.

2.1.1. Sensitizing and activating treatment

The sensitizing solution was produced by dissolving 2.5 g $SnCl_2$ into 0.1 M HCl solution. This solution was aged for 3 days before it was used, for improving its sensitizing performance due to the formation of uniform colloidal compound of Sn(IV) and Sn(II) [14]. The activating solution consists of 2.82 mM $PdCl_2$ and 0.1 M HCl. Vulcan XC-72 carbon blacks were ultrasonicated in the sensitizing solution for 30 min at room temperature, centrifugated, and immersed in deionized water in ultrasonic bath. Then, the sensitized particles were transferred into the activating solution and ultrasonicated for 30 min, with the color change of the solution from yellow to achromatic because of the reduction of Pd(II) ion. After pretreatment, the carbon particles were transferred into the deposition bath containing hexachloroplatinic acid and ruthenium chloride for the deposition of metal particles.

2.1.2. Deposition process

First, Vulcan XC-72 carbon blacks were mixed with certain amount of H_2PtCl_6 (1.93 mM) and $RuCl_3$ (3.63 mM) solution, the molar ratio of Pt and Ru is 1:1. After 1 h of vigorous stirring at room temperature, Na_2CO_3 solution was added to the above mixture until it reached a pH value of 10. A borohydride sodium solution (20 mg L^{-1}) as a reducing agent was then added into the slurry dropwise. The resulting suspension was maintained under constant stirring at room temperature for 2 h to allow a complete reduction of Pt and Ru. Subsequently, the mixture was centrifugated and washed thoroughly with deionized water to remove chlorine ions. The final catalyst was dried in a vacuum oven at 60 °C for 6 h.

PtRu/C (Pt/Ru = 1:1 a.t.) catalysts with 20 wt.% Pt loading prepared by electroless deposition with and without pretreatment were labeled as catalysts **A** and **B**, respectively. Those with low Pt loading (15 wt.%) obtained with and without pretreatment were signed as catalysts **C** and **D**, respectively.

2.2. Characterization and electrochemical measurement

The structure of the obtained samples was characterized by powder X-ray diffraction (XRD, Janpan Rigaku D/max 2500 X-ray generator with graphite monochromatized Cu Kα radiation, λ = 1.5406 Å) at a scanning rate of 4° min^{-1} from 3° to 80°. Transmission electron microscope (TEM) and high resolution TEM (HRTEM) images were obtained using a Philips Tecnai F20 system operated at 200 kV. Energy dispersive X-ray (EDX) was performed in the JEOL JSM-5600 scanning electron microscope using of a Kevex Super 8000 detector working at an accelerating voltage of 20 kV.

Electrochemical measurements were carried out with electrochemical workstation (EG&G Princeton, Model 2273) using a conventional three-electrode electrochemical cell at 25 °C. A glassy carbon (GC) was employed as the working electrode, a Pt flake of 1 cm^2 area was used as the counter electrode, and Ag/AgCl (saturated KCl) electrode was applied as the reference electrode. All potential values were referenced to Ag/AgCl. Before each experiment, the GC electrode was polished with alumina nanaoparticles slurry to a mirror. Five milligrams of the as-prepared PtRu/C catalysts were added into the solution containing 0.5 mL of 5% Nafion and 0.5 mL ethanol, which was ultrasonicated for 1 h to get homogeneous slurry. Then, 5 μL of the slurry was dropped on the mirror-polished GC electrode with 3 mm diameter. Subsequently, the electrode was dried at 60 °C for 1 h. The cyclic voltammetry (CV) measurements were carried out in 0.5 M H_2SO_4 electrolyte at the scan rate of 20–50 mV s^{-1} or in the electrolyte consisting of 0.5 M H_2SO_4 and 1 M methanol at room temperature. To obtain chronoamperometry curves, the working electrode was polarized at 0.5 V in the above mentioned solution for 1500 s. Before each test, the solution was purged with N_2 for 15 min.

3. Results and discussion

3.1. XRD analysis

Fig. 1 shows the XRD patterns of the two PtRu/C samples obtained by the electroless deposition method with (catalyst **A**) and without (catalyst **B**) the pretreatment of sensitization and activation. The broad peak at low angle (near $2\theta = 24.5°$) is attributed to the diffraction of the carbon support. For both catalysts, the characteristic diffraction peaks of PtRu particles can be indexed to the (1 1 1), (2 0 0) and (2 2 0) reflections of a Pt face-centered cubic (fcc) crystallographic structure and no visible peaks related to RuO_2 or Ru can be found [15]. It is noted that

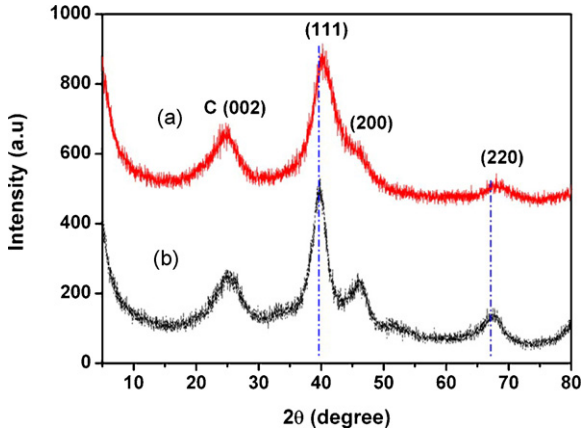

Fig. 1. XRD patterns of PtRu/C catalysts: (a) catalyst **A** and (b) catalyst **B**.

a slight shift of 2θ towards higher values was observed and that the shifts in 2θ for catalyst **A** are higher than that of catalyst **B**. For example, the peak of (1 1 1) diffraction of **A** is at $2\theta = 40.3^\circ$, whereas it is 39.8° for **B**. This is probably because more Ru atoms incorporate into the Pt crystal lattice during the formation of alloy metal particles [16]. Accordingly, the alloying degree of PtRu for **A** is higher than that for **B**, which may be favorable for the catalytic performance in methanol electrooxidation.

The lattice constants of the **A** and **B** catalysts are 3.886 and 3.911 Å, respectively, which are smaller than that (3.916 Å) of carbon supported pure Pt [16]. The reduction of lattice constant further confirms the formation of PtRu alloy in catalysts. In addition, all diffraction peaks are broadened and no sharp diffraction peak can be observed in the as-synthesized catalysts, indicating small grain size or poor crystalline degree of the products. The peaks of catalyst **A** are a little broader than those of **B**, which denotes that **A** possesses smaller particle size than that of **B**. The average particle size of the obtained catalysts is calculated from Scherrer formula (Eq. (1)) [15]:

$$D = \frac{0.9\lambda_{K\alpha_1}}{B_{1/2}\cos\theta_{max}} \quad (1)$$

where D is the average particle size, $\lambda_{K\alpha_1}$ the wavelength of the incident X-ray (Cu $K\alpha_1 = 1.5406$ Å), $B_{1/2}$ the half-height width at peak maximum and θ is the Bragg diffraction angle in radian unit. Based on the (2 2 0) peaks, the average particle sizes for catalysts **A** and **B** are 3.5 and 4.0 nm, respectively.

3.2. TEM characterization

Fig. 2 displays the representative TEM images and size distribution histograms of catalysts **A** and **B**. As shown in Fig. 2a, the nanoparticles of catalyst **A** are well dispersed on the carbon support and the particle size is uniformly distributed without any aggregation. The insets of Fig. 2a and b show the corresponding HRTEM micrograph of a single particle, giving the interlaced lattice fringes of the PtRu alloy with somewhat defects. In addition, the nanoparticles of catalyst **A** exhibit a relatively narrow size distribution of 2–5 nm, with approximately 50% of them centered at 3.2 nm (Fig. 2c). In comparison, a number of nanoparticles of catalyst **B** appear to congregate, as shown in Fig. 2b. The particle sizes of **B** are in the range of 1.5–7 nm, with the average particle size around 4.0 nm (Fig. 2d). Hence, the PtRu nanoparticles synthesized with sensitizing and activating pretreatment possess smaller average particle size and they are better dispersed on the carbon support. The particle size of both catalysts observed from TEM measurement further confirms the calculated result from XRD analysis.

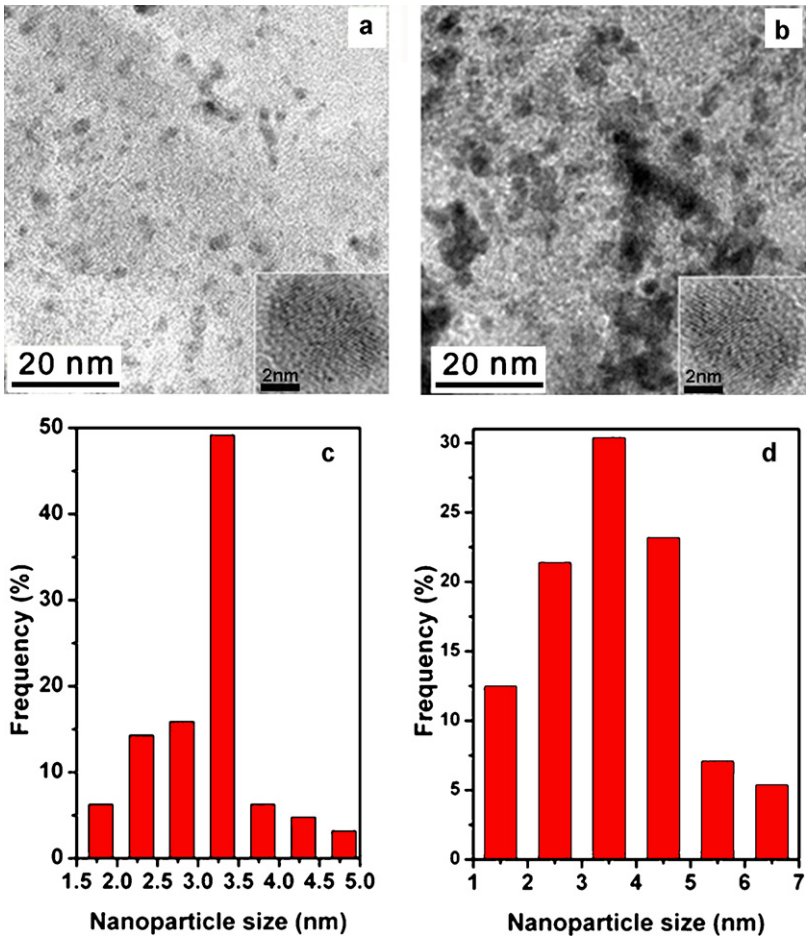

Fig. 2. Typical TEM images and particle size distribution of PtRu/C catalysts prepared by an electroless deposition route with (catalyst **A**, a and c) and without (catalyst **B**, b and d) the pretreatment of sensitization and activation. The inset shows the corresponding HRTEM micrograph of an individual nanocrystal.

3.3. Proposed mechanism of PtRu/C formation

The different characterization results of the two catalysts fabricated by electroless deposition method with and without the sensitizing and activating treatment can be explained by the following anchoring deposition mechanism. Because of the interfacial tension of hydrophobic carbon surface, it is difficult for $PtCl_6^{2-}$ to adsorb onto the surface of carbon support. Most of the $PtCl_6^{2-}$ and Ru^{3+} ions are reduced to free nanoparticles in solution rather than on carbon surface. These free nanoparticles are unstable and prone to aggregate into bulk metal particles. Such a conglomeration leads to poor dispersion of metal particles, which can be detected from TEM measurement (Fig. 2b).

For sensitizing treatment, Sn(II) and Sn(IV) colloidal ions adsorbed on the hydrophobic carbon surface can provide a path for the adsorption of ions on the carbon substrate through electrostatic interactions [17]. While for activating treatment, Pd particles on the carbon surface serve as micro-reactors for the reduction of metal particles. Pd nucleus on carbon surface can catalyze the reaction of $NaBH_4$ in alkaline solution, which is essential for the reduction of Pt(IV) and Ru(III). As a result, most PtRu metal particles are deposited on carbon surface with small particle size and narrow size distribution.

$$Sn_{ad}^{2+} + Pd_{ad}^{2+} \rightarrow Pd_{ad}^{0} + Sn^{4+} \quad (2)$$

$$2Pd^{0} + PtCl_6^{2-} \rightarrow 2Pd^{2+} + Pt^{0} + 6Cl^{-} \quad (3)$$

$$8PtCl_6^{2-} + 8Ru^{3+} + 7BH_4^{-} + 56OH^{-} \rightarrow 8Pt^{0}Ru^{0} + 7B(OH)_4^{-} + 28H_2O + 48Cl^{-} \quad (4)$$

3.4. EDX analysis

The composition of catalyst **A** was determined by energy-dispersive X-ray (EDX) analysis. Fig. 3 shows the representative EDX spectra for catalyst **A**. The existence of elemental Pt and Ru can be seen clearly, and no specific spectra of Sn and Pd are observed, confirming that the excessive Sn(II) and Pd(0) formed in the procedure of sensitization and activation are removed completely. The average Pt/Ru atomic ratio of the catalyst **A** is 0.51:0.49, which is almost the same as the expected value of

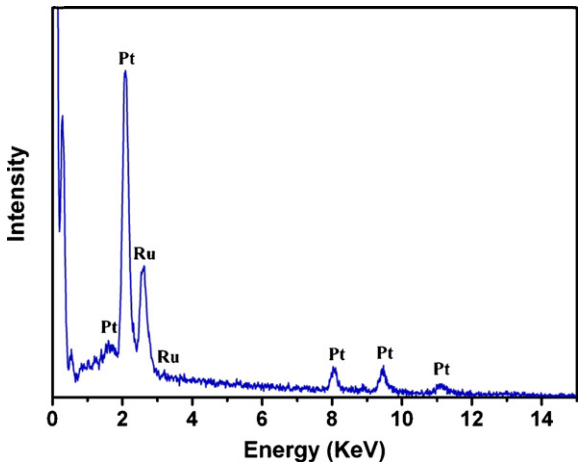

Fig. 3. Representative EDX spectra of catalyst **A**.

Pt/Ru atomic ratio of 1:1. Furthermore, EDX measurements are taken several times randomly on different areas of the sample. All tests have the uniform atomic composition of Pt and Ru, revealing homogenous distribution of the catalyst.

3.5. Electrochemical measurement

The electrochemical active surface areas (EAS) of the as-synthesized catalysts were determined by CV measurement performed in 0.5 M H_2SO_4 electrolyte without methanol at a scan rate of 50 mV s^{-1}. The typical voltammograms are shown in Fig. 4a (for catalysts **A** and **B**) and 4b (for catalysts **C** and **D**), in which all anodic limits are 1.2 V versus that of a reference electrode Ag/AgCl. The hydrogen adsorption/desorption peaks are clearly shown in the voltammograms at potentials from −0.2 to 0.1 V and the cathodic peak of Pt oxide reduction at around 0.45 V. In Fig. 4a, it can be observed that the hydrogen adsorption/desorption peak of catalyst **A** is larger than that of catalyst **B**, which demonstrates that catalyst **A** has more active Pt sites than catalyst **B**, although they have the same elemental composition and metal loading. In Fig. 4b, catalyst **C** exhibits larger hydrogen adsorption/desorption peak than that of catalyst **D**, which means that catalyst **C** has a relative larger electrochemical active surface area in comparison with catalyst **D**. This CV measurement shows that sensitizing and activating pretreatment

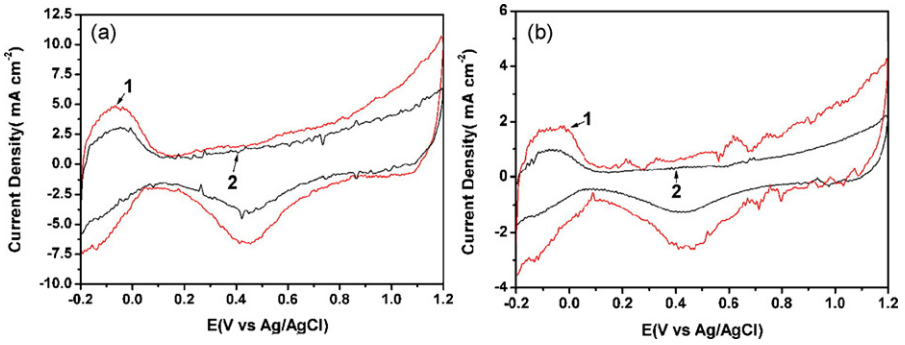

Fig. 4. Cyclic voltammograms of catalyst **A** (red) and **B** (black) (a), catalyst **C** (red) and **D** (black) (b) on glassy carbon electrode in 0.5 M H_2SO_4 solution at 25 °C, at a scan rate of 50 mV s^{-1}. (For interpretation of the references to color in this figure legend, the reader is referred to the web version of the article.)

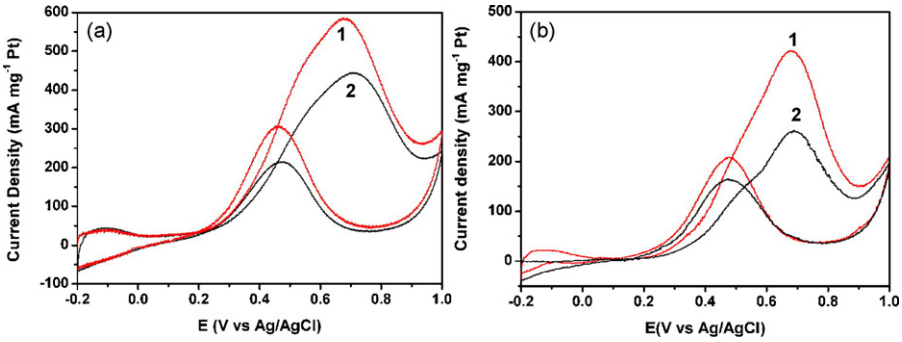

Fig. 5. Clyclic voltammograms of catalyst **A** (red) and **B** (black) (a), catalyst **C** (red) and **D** (black) (b) on glassy carbon electrode in 1 M methanol + 0.5 M H_2SO_4 solution at 25 °C, at a scan rate of 20 mV s^{-1}. (For interpretation of the references to color in this figure legend, the reader is referred to the web version of the article.)

promotes the dispersion of metal particles on the carbon support, which is favorable for the electrocatalytic performance of the catalysts. The electrochemical active surface area of the two catalysts can be calculated from the CV curves by the following equation [18].

$$S = \frac{Q}{L_{Pt} q_H^0} \tag{5}$$

Q is the integrated area of the hydrogen desorption (μC), L_{Pt} the loading of Pt on the working electrode (mg), and q_H^0 is the charge for monolayer hydrogen adsorption on Pt 2 1 0 (μC cm^{-2}). The electrochemical active surface areas of catalysts **A**–**D** are 72.3, 56.2, 47.4 and 32.3 m^2 g^{-1}, respectively.

The catalytic activities for methanol oxidation of catalyst **A**–**D** were characterized by cyclic voltammerty (CV) performed in the electrolyte consisted of 0.5 M H_2SO_4 and 1 M methanol. The results are shown in Fig. 5. The currents were normalized to the amount of Pt loading on the synthesized catalysts. It is observed from curve 1 in Fig. 5a that during the forward scan, the onset potential (E_{onset}) of methanol oxidation for catalyst **A** is 0.22 V. The current density increases rapidly with potential and reaches a specific peak current density (C_{pa}) of 589.9 mA mg^{-1} at 0.67 V (E_{pa}). This peak is attributed to the oxidation of methanol on catalyst surfaces. During the reverse scan, the peak current density is 312.6 mA mg^{-1} at 0.44 V, which can be ascribed to the reduction of the oxidized Pt oxide and the oxidation of methanol and intermediates [19]. For catalyst **B**, curve 2 in Fig. 5a, the onset and peak potentials of methanol oxidation are observed at 0.28 and 0.71 V, respectively, which are more positive than the corresponding values of **A**. The peak on the reverse scan is centered at 0.47 V with a current density of 215.7 mA mg^{-1}. The peak current on forward scan of methanol oxidation for catalyst **A** is about 34% higher than that of **B**.

Fig. 5b shows the voltammogram of methanol oxidation on catalysts **C** and **D**. For catalyst **C** (curve 1 in Fig. 5b), the onset of methanol oxidation occurs at 0.28 V and the current density reaches at the maximum of 421 mA mg^{-1} Pt at around 0.69 V during the forward scan. The peak current on reverse scan is observed at 0.48 V and the corresponding current density is 208 mA mg^{-1} Pt. While, for catalyst **D** (curve 2 in Fig. 5b), the onset potential is 0.3 V and the peak current density of 260 mA mg^{-1} Pt occurs at about 0.71 V, the reverse scan current density reaches at peak at about 0.49 V with the corresponding current density of 170 mA mg^{-1} Pt. The peak current density for methanol oxidation on catalyst **C** is about 1.6 times as that of catalyst **D**. Furthermore, a phenomenon should be noted that catalytic activity for catalyst **C** (curve 1 in Fig. 5b) is comparable to that of catalyst B (curve 2 in Fig. 5a) in the CV measurement, although the noble metal loading of catalyst **C** is lower than that of catalyst **B**.

In order to investigate the long-term performance of the obtained PtRu/C catalysts towards the methanol oxidation reaction, chronoamperometry tests were carried out in 1 M CH_3OH solution containing 0.5 M H_2SO_4. The chronoamperometric responses at a constant potential of 0.5 V are given in Fig. 6. As shown in the figure, all curves exhibit the similar trend that current densities decay rapidly with time in the initial stage and

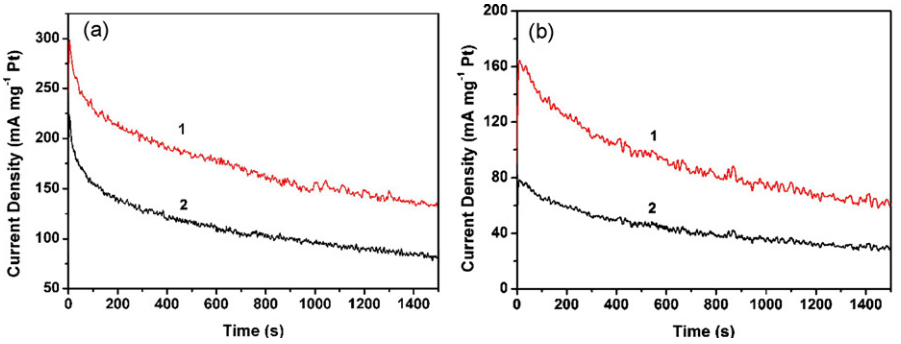

Fig. 6. Chronoamperometry curves for catalyst **A** (red) and **B** (black) (a), catalyst **C** (red) and **D** (black) (b). Polarization at 0.5 V in a solution containing 1 M methanol and 0.5 M H_2SO_4. (For interpretation of the references to color in this figure legend, the reader is referred to the web version of the article.)

Table 1
Comparison activity of the as-synthesized catalysts

	Pt loading (wt.%)	E_{onset} (V)	C_{pa} (mA mg^{-1})	E_{pa} (V)	EAS (m^2 g^{-1})	C_{600} (mA mg^{-1})
Catalyst **A**	20	0.22	589.9	0.67	72.3	177.1
Catalyst **B**	20	0.28	444.2	0.71	56.2	109.8
Catalyst **C**	15	0.28	421.0	0.69	47.4	92.0
Catalyst **D**	15	0.30	260.0	0.71	32.3	43.2

decreases gradually for a long operation time. It is noted that catalyst **C** (with 15% metal loading) declined slightly faster than that of catalyst **D** in the preliminary stage (in the initial 600 s). But, the declining rate went down with time. After 800 s, the current density declines slightly, and maintains a relatively stable value. During the whole chronoamperometry polarizing test, the current density of catalyst **C** is higher than that of catalyst **D**. The current decay may be ascribed to the formation and adsorption of intermediate species on the active sites of the catalysts. It is noted in Fig. 6a that catalyst **A** maintains a relative higher current than catalyst **B**, which indicates the better catalytic performance of **A** for methanol oxidation. The response for catalysts **C** and **D** is shown in Fig. 6b, and a similar-shaped chronoamperometry is also shown. The current density of catalyst **C** is much higher than that of **D**, which indicates that the long-term performance of catalyst **C** is better than **D**. Hence, the result of chronoamperometry tests agrees with the cyclic voltammograms measurement. As a result, the comparison activities of the as-synthesized four catalysts are summarized in Table 1.

Both cyclic voltammetry measurement (CV) and chronoamperometry results indicate that at the same Pt loading, catalysts synthesized by electroless deposition with the sensitizing and activating pretreatment are more active in electro-catalyzing the methanol oxidation reaction compared to those obtained by electroless deposition without pretreatment. Also, the catalytic activity for methanol oxidation of catalyst **C** is comparable to that of **B**, although the Pt loading of catalyst **C** is lower than **B**. Therefore, the sensitizing and activating treatment during the electroless deposition synthesis plays an important role in the catalytic performance of PtRu/C catalyst in our study. The improved catalytic activity by the pretreatment of sensitization and activation is attributed to the smaller particle size, narrower size distribution, better dispersion of nanoparticles on carbon support, as well as the relatively higher alloy degree of PtRu particles.

4. Conclusions

In conclusion, well dispersed PtRu/C catalysts with high catalytic performance for methanol oxidation reaction were successfully prepared by an electroless deposition method with the pretreatment of sensitization and activation. Morphology and composition analysis showed that the as-synthesized PtRu nanoparticles were deposited on carbon support with better dispersion, narrower particle size distribution, higher alloying degree than that obtained without pretreatment. Electrochemical measurement demonstrated that the PtRu/C catalyst obtained with the sensitizing and activating pretreatment exhibited an improved catalytic activity (approximately 34% enhanced current density) for methanol electrooxidation. The enhanced catalytic performance was supposed to derive from the favorable morphology and composition of the catalyst.

Acknowledgements

This work was supported by the National NSFC (90406001), Ministry of Education (2004164) and TJKJ (05YFJMJC00300).

References

[1] E. Reddington, A. Sapienza, B. Gurau, R. Viswanathan, S. Arangapani, E.S. Smotkin, T.E. Mallouk, Science 280 (1998) 1735.
[2] T. Shimizu, T. Momma, M. Mohamedi, T. Osaka, S. Sarangapani, J. Power Sources 137 (2004) 277.
[3] J. Chen, Z.L. Tao, S.L. Li, J. Am. Chem. Soc. 126 (2004) 3060.
[4] T.C. Deivaraj, J.Y. Lee, J. Power Sources 142 (2005) 43.
[5] K. Miyazaki, K. Matsuoka, Y. Iriyama, T. Abe, Z. Ogumi, J. Electrochem. Soc. 152 (2005) A1870.
[6] L.S. Sarma, T.D. Lin, Y.W. Tsai, J.M. Chen, B.J. Hwang, J. Power Sources 139 (1–2) (2005) 44.
[7] Z. Jusys, T.J. Schmidt, L. Dubau, K. Lasch, L. Jorissen, J. Garche, R.J. Behm, J. Power Sources 105 (2002) 297.
[8] M. Watanabe, S. Motoo, J. Electroanal. Chem. 60 (1975) 267.
[9] T. Frelink, W. Visscher, J.A.R. van Veen, Surf. Sci. 335 (1995) 353.
[10] Y.W. Tang, L.L. Zhang, Y.N. Wang, Y.M. Zhou, Y. Gao, C.P. Liu, W. Xing, T.H. Lu, J. Power Sources 162 (2006) 124.
[11] Y.H. Lee, G. Lee, J.H. Shim, S. Hwang, J. Kwak, K. Lee, H. Song, J.T. Park, Chem. Mater. 18 (2006) 4209.
[12] Y. Su, X.Z. Xue, W.L. Xu, C.P. Liu, W. Xing, X.C. Zhou, T. Tian, T.H. Lu, Electrochim. Acta. 51 (2006) 4316.
[13] Z. Chen, P. Zhan, Z.L. Wang, J.H. Zhang, W.Y. Zhang, N.B. Ming, C.T. Chan, P. Sheng, Adv. Mater. 16 (2004) 417.
[14] Z.L. Liu, X.H. Lin, J.Y. Lee, W. Zhang, M. Han, L.M. Gan, Langmuir 18 (2002) 4054.
[15] J.W. Guo, T.S. Zhao, J. Prabhuram, R. Chen, C.W. Wong, Electrochim. Acta. 51 (2005) 754.
[16] E. Antolini, F. Cardellini, J. Alloys Compd. 315 (2001) 118.
[17] N. Feldstein, J.A. Weiner, J. Electrochem. Soc. 120 (1973) 475.
[18] R.Z. Yang, X.P. Qiu, H.R. Zhang, J.Q. Li, W.T. Zhu, Z.X. Wang, X.J. Huang, L.Q. Chen, Carbon 43 (2005) 11.
[19] W.L. Xu, T.H. Lu, C.P. Liu, W. Xing, J. Phys. Chem. B 109 (2005) 14325.